Diagnosing Alzheimer's Disease and Discriminating Between Its Stages from Brain FDG PET Images Using a New Platform for Radiomic Analysis

Ramin Rasi * and Albert Guvenis

Posted Date: 8 November 2023

doi: 10.20944/preprints202311.0513.v1

Keywords: Alzheimer's disease (AD); Mild Cognitive Impairment (MCI); FDG PET; Radiomics

Article

Diagnosing Alzheimer's Disease and Discriminating between Its Stages from Brain FDG PET Images Using a New Platform for Radiomic Analysis

Ramin Rasi [1,*], Albert Guvenis [1] and for the Alzheimer's Disease Neuroimaging Initiative [†]

[1] Institute of Biomedical Engineering Boğaziçi University, Türkiye; guvenis@boun.edu.tr
* Correspondence: Raminrasi@yahoo.com
† Data used in preparation of this article were obtained from the Alzheimer's Disease Neuroimaging Initiative (ADNI) database (adni.loni.usc.edu). As such, the investigators within the ADNI contributed to the design and implementation of ADNI and/or provided data but did not participate in analysis or writing of this report. A complete listing of ADNI investigators can be found at: http://adni.loni.usc.edu/wp-content/uploads/how_to_apply/ADNI_Acknowledgement_List.pdf.

Abstract: This study presents a methodological framework for AD and MCI diagnosis using radiomic analysis of 18FDG-PET imaging and conducts non-invasive predictions ~~and in-depth analysis~~ of AD and MCI and the associated small number of regions and features. Our methodology follows a structured process commencing with data preprocessing and labeling, facilitating segmentation through FastSurfer, a tool that efficiently segments the brain into 95 ROIs using the DKT-atlas. Subsequently, Feature extraction was carried out using PyRadiomics, calculating 120 features for each of the 95 ROIs (11,400 per image). These extracted features form the foundation of our radiomics analysis, primarily for early diagnostic purposes. In the feature selection phase, we explored a set of eight commonly employed techniques, including ANOVA, PCA, and LASSO, originating from the four main categories, namely filtered, embedded, wrapper, and hybrid methods, to identify a pertinent subset of features. Our evaluation assessed the performance of nine classification methods, such as GradientBoosting, RandomForest, and GaussianNB, in conjunction with eight feature selection techniques. The choice of feature selection method and classifiers was predicated on their ability to achieve the best area under the ROC curve with independent data. For all three predictions AD vs. CN, AD vs. MCI, and CN vs. MCI the Random Forest (RF) classifier with LASSO feature selection demonstrated the highest accuracy with an AUC of 0.976 for AD vs CN, AUC=0.917 for AD vs MCI, and AUC=0.877 for MCI vs CN. In conclusion, our RAB-PET platform enables efficient AD and MCI diagnosis from FDG-PET images using a radiomics pipeline. It also offers a general hardware and software tool for the investigation of other brain disorders.

Keywords: Alzheimer's disease (AD); mild cognitive impairment (MCI); FDG PET; radiomics

1. Introduction

Alzheimer's disease (AD), the most common progressive neurological disease among elderly individuals, is a neuropsychiatric disorder that causes many economic and psychological difficulties for the patient's community and family[1]. According to the estimation of WHO the number of people with age over the 60 years old will reach to 2.1 billion people by 2050[2]. In a study researchers show that Alzheimer's disease starts building up in the brain long before symptoms appear[3], so it is possible to detect this pathology in vivo using biomarkers such as molecular imaging techniques in the early stage of formation[4]. Conversely, the challenge of identifying Alzheimer's disease (AD) in its initial stages remains a prominent concern in its treatment. Given the intricate nature of AD as a gradual, multifaceted ailment, healthcare professionals employ an array of clinical assessments and neuroimaging methods in their endeavors to detect dementia during its early phases. This is a crucial aspect of managing the disease effectively[5,6]. Advanced imaging techniques play a pivotal role in the timely identification of medical conditions and contribute significantly to the development of tailored treatment approaches within the realm of precision medicine. These techniques not only enhance the ability to detect diseases at their early stages but also facilitate the delineation of novel therapeutic

 doi:10.20944/preprints202311.0513.v1

strategies that are customized to individual patients, leading to more effective and personalized healthcare[7]. In the present work, we hypothesize that we can predict different stages of AD noninvasively from 18FDG-PET images using a radiomic analysis platform. There have been studies to predict AD from various biomarkers that can provide early information on the pathology of the disease before even symptoms occur[8]. Over the past few years, there have been notable advancements in the utilization of radiomics in conjunction with machine learning (ML) and deep learning (DL) techniques for the analysis of medical images as data. In the realm of machine learning, a substantial quantity of manually crafted features that describe various aspects of medical images are extracted. These features are then scrutinized to discern their associations with patient prognosis and other relevant attributes[9]. Radiomic methods try to extract visible and invisible information from medical imaging using various computations on different regions. It has been introduced as an effective solution to deduce a number of disease characteristics using a high number of low-level imaging features as an extension of computer-assisted medical decision support (CMD) systems [10,11].

The radiomics approach encompasses a sequence of distinct stages, including image acquisition, image processing, delineation of regions of interest or volumes of interest (ROI/VOI), extraction of relevant features, feature selection, and the development of classification or regression models. These methods can employ manual, semi-automated, or fully automated delineation algorithms. However, manual and semi-automated segmentation methods are influenced by individual users, potentially making the extracted features within the ROI/VOI susceptible to variations caused by both intra- and interobserver discrepancies. Consequently, the adoption of artificial intelligence and deep learning techniques for automated segmentation, aimed at mitigating the impact of subjective biases, stands out as a critical and indispensable domain of radiomics research [12]. In order to streamline and mechanize the procedure, we have integrated FastSurfer[13] into our workflow for volumetric analysis. FastSurfer is a tool that emulates the anatomical segmentation method employed by FreeSurfer[14], enabling us to divide the entire brain into 95 distinct categories by utilizing the DKT-atlas.

The primary objective of this research is to develop a tailored platform for the radiomic analysis of FDG-PET brain images, facilitating the noninvasive extraction of quantitative data to assist in diagnosing and tailoring treatment for individual patients. We posit that our platform represents a new initiative, allowing for the generation of multiple outcomes using specialized hardware. To evaluate its efficacy, we initially apply the system to data from Alzheimer's disease (AD) patients obtained from an online database. Subsequent sections detail the methodologies employed, the findings obtained, their implications, and the resulting conclusions.

This study builds upon our previous research[15], aiming to both continue and broaden our investigation. In this updated study, by extending our focus to include individuals with mild cognitive impairment (MCI). Moreover, we perform a comprehensive analysis of various brain regions associated with both Alzheimer's and MCI.

2. Literature review

The development of an interpretable model for the prediction of Mild Cognitive Impairment (MCI) and Alzheimer's Disease (AD) represents a formidable challenge that has garnered substantial attention in the research community. In this study, we contribute to this ongoing endeavor by presenting a predictive model for MCI and AD, wherein we identify significant brain regions, drawing support from prior research[16–18] and highlighting the importance of the amygdala[19]. Here we present a few significant and recent studies. A more comprehensive summary in the form of a table is given in the discussion section.

A pivotal study[20] leveraged two distinct imaging techniques, FDG PET and MRI, to predict the presence of MCI and AD, comparing them to normal controls (CN) through the application of radiomics. Their results were quite promising, achieving an impressive AUC of 0.98 for distinguishing AD from CN and an AUC of 0.85 for discerning MCI from CN. Notably, the study employed LASSO feature selection on characteristics extracted from the hippocampus and utilized a logistic regression model with cross-validation (CV=5). These findings suggest that information derived from the hippocampus could serve as a valuable biomarker for investigating Alzheimer's

 doi:10.20944/preprints202311.0513.v1

disease within clinical contexts. This corroborates our own research, which underscores the significance of the hippocampus (rh) as one of the top three crucial regions closely associated with AD and MCI.

In a separate meta-analysis study[21], researchers investigated the potential of machine learning (ML) algorithms to aid in the automated detection and diagnosis of diseases, with a special focus on the detection of Alzheimer's disease using medical imaging as a non-invasive biomarker. Their analysis encompassed 24 distinct ML models from 19 research papers, covering various brain regions. The achieved AUC of 0.93 demonstrates the high accuracy of ML in distinguishing Alzheimer's disease from normal controls. The study also highlights the prevalence of internal validation as a limitation in the field, a concern raised in another study[22] ,where only 6% of the 516 reviewed studies utilized external validation. This meta-analysis underscores the remarkable performance of ML in diagnosing AD, while also emphasizing the need for high-quality, large-scale prospective studies to enhance its reliability and applicability in clinical practice.

Another noteworthy investigation[23] ,proposed a model to predict the progression of MCI to AD using FDG PET images, based on a radiomics approach. This study focused on white matter and constructed an integrated model, applying it to features extracted from this region. The research revealed the association of white matter with MCI progression to AD and highlighted differences between two groups of patients with stable and progressing MCI. Notably, FDG PET was found to significantly improve the prediction of MCI to AD progression compared to MRI and cerebrospinal fluid analysis, as supported by[24]. This study opted for FDG PET due to its cost-effectiveness and ease of implementation in contrast to other radiotracers used to measure TAU and Amyloid proteins. Furthermore, the study introduced the psycho-radiomics model, which combines FDG PET features with clinical data to identify high-risk MCI patients.

Recent research underscores the significant challenge within radiomics studies, which involves successfully integrating algorithms with suitable biomarkers. The selection of new and performing algorithms at various stages of radiomics is critical, and the identification of pertinent biomarkers has been a central focus in recent investigations. Furthermore, there is a persistent emphasis on elucidating characteristics that can be easily understood, as well as a keen interest in the interpretability of results, given the need to transform these findings into actionable insights.

In comparison to recent studies, our platform not only yields very accurate results but also imparts valuable insights by identifying more efficient brain regions, all without any prior preconceived notions or existing knowledge about these areas. Furthermore, we introduce interpretable features specific to each stage of Alzheimer's disease. The developed hardware and software platform is designed to be flexible so that it can be used to address various issues related to neurological disorders of the brain. We incorporated recent methods for image segmentation, feature selection, and classification. The sole reliance on FDG PET as a biomarker in our research underscores our method's advantage as an economical and non-invasive approach.

3. Method

Our methodology involves systematic steps, beginning with pre-preprocessing and labeling the data. We then extract regions of interest (ROIs) using FastSurfer. Feature extraction follows, where we compute 120 features from 18FDG-PET images. These features underpin our radiomics analysis for early diagnosis and interpretation. Subsequent sections delve into each step's details.

3.1. ADNI and Participants

Data used in the preparation of this article were obtained from the Alzheimer’s Disease Neuroimaging Initiative (ADNI) database (adni.loni.usc.edu). The ADNI was launched in 2003 as a public-private partnership, led by Principal Investigator Michael W. Weiner, MD. The primary goal of ADNI has been to test whether serial magnetic resonance imaging (MRI), positron emission tomography (PET), other biological markers, and clinical and neuropsychological assessment can be combined to measure the progression of mild cognitive impairment (MCI) and early Alzheimer’s

Preprints (www.preprints.org) | NOT PEER-REVIEWED | Posted: 8 November 2023 doi:10.20944/preprints202311.0513.v1

disease (AD). Detailed information about the participants' clinical characteristics can be found in Table 1.

Table 1. Clinical characteristics of participants

Clinical Diagnosis	No. Cases	Sex (M/F)	Age (mean ± SD)
AD	163	91/72	74.6 ± 8.12
MCI	198	107/91	72.5 ± 8.07
CN	188	91/97	73.6 ± 6.37
Total	549	289/260	74.1 ± 7.02

3.2. PET Acquisition.

The 18-fluoro-deoxyglucose PET imaging data, obtained during the initial visit to the ADNI database, were furnished in two forms: raw and preprocessed, and then categorized into four distinct groups based on the applied preprocessing procedures, as detailed on adni.loni.usc.edu. These data consisted of dynamic 3D scans, with a radiotracer dosage of 185 MBq (5 mCi), comprising six 5-minute frames captured between 30 to 60 minutes post-injection. For our analysis, we specifically utilized the third type of preprocessed 18FDG-PET image data, characterized by Co-Reg, AVG, Standardized Image, and Voxel Size adjustments. Within this dataset, the 18FDG-PET images were adjusted to adhere to a standardized 160×160×96 voxel imaging grid, with each voxel measuring 1.5 mm on all sides, as referenced in[25].

3.3. ROI Extraction

The pursuit of efficiency and speed in handling large datasets has driven the evolution of more robust tools and methods. In this endeavor, we harnessed the capabilities of FastSurfer, a tool that significantly expedites volumetric analysis. This tool emulates the anatomical segmentation method employed by FreeSurfer, allowing for the comprehensive division of the entire brain into 95 distinct classes. This segmentation process, guided by the DKT-atlas, is illustrated in Figure 1. By adopting FastSurfer, we've streamlined the process, enabling swift and precise analysis of brain structures, which is critical for our radiomics approach's success.

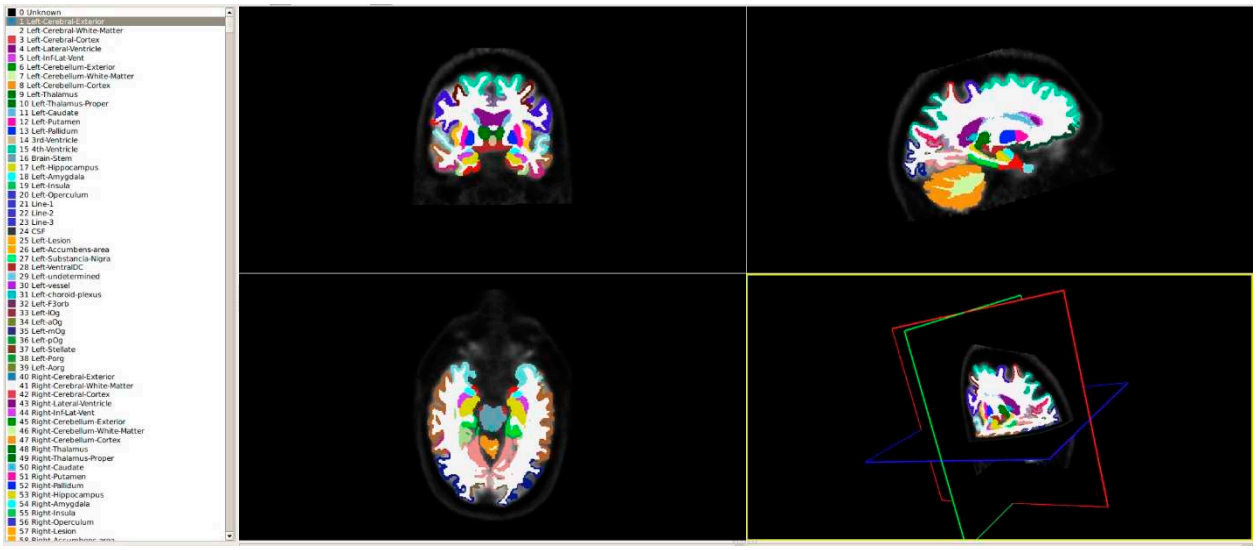

Figure 1. Visualization of the brain segmentation into 95 regions of interest using DKT-Atlas.

3.4. Feature Extraction

 doi:10.20944/preprints202311.0513.v1

To extract the features from 18FDG-PET, we used an open-source python package: PyRadiomics[26]. We calculated 120 feature classes: first-order statistics (19), gray level dependence matrix (14), shape-based (2D) (10), gray level cooccurrence matrix (24), gray level run length matrix (16), neighboring gray tone difference matrix (5), gray level size zone matrix (16 features) and shape-based (3D) (16). All features were computed from the extracted 95 ROIs in 18FDG-PET images.

3.5. Feature Selection

In the realm of radiomics research, feature selection is crucial for condensing the extensive array of features derived from available datasets[27,28] and for improving performance. Our evaluation encompassed a comprehensive study of the effectiveness of various feature selection techniques, including filtered, embedded, wrapper, and hybrid methods, each holding their distinct advantages[29]. To ensure the robustness of our approach, we opted for widely used algorithms from each category[30–32]. These encompassed ANOVA, PCA, chi-square, LASSO, MI, RFA, FI, and RFE among others[33], all lly considered to identify the most pertinent subset of features for our radiomics analysis.

3.6. Classification and Tuning

Researchers have developed a range of classification methods[34] and identifying the most suitable machine-learning approach for radiomics applications is a pivotal phase, with high-performing classifiers contributing significantly to the enhancement of clinical applications based on radiomics. In our investigation, we assessed the performance of nine classification methods, spanning various classifier families, including GradientBoosting (GB), RandomForest (RF), DecisionTree (DT), GaussianNB (GNB), GaussianProcess (GP), MLP, QuadraticDiscriminantAnalysis (QDA), AdaBoost (AB), and KNeighbors (KNN), in conjunction with eight different feature selection techniques. This exhaustive analysis, resulting in 72 distinct combinations of classification methods and feature selection methods, led to the selection of classifiers that exhibited the most favorable area under the ROC curve for our proposed solution. This selection process was executed with default parameters as stipulated in the Scikit-learn library, and we also paid close attention to the critical task of hyperparameter optimization. To achieve this, we conducted randomized search cross-validation (CV=5) tuning using 70% of the data, reserving 30% for independent testing, and iterated this process 100 times under completely random conditions[35,36].

3.7. Computational hardware and software

The hardware that was used for the RAB-PET platform was the Corei7 Gen10th processor, RTX2060 VGA card (1920 CUDA cores with 240 tensors), and 16 GB DDR5 RAM. We used Python as a programming language and PyTorch to utilize the CUDA technology. We used FastSurfer components to segment the brain using a deep learning approach and PyRadiomics components to extract features under IBSI[37,38]. Phyton libraries were used to come up with a reduced set of features that can be used as input to our prediction model. The code for the prediction model can be found in Zendo data repository[39].

4. Results

In this research, we conducted predictions in three distinct categories: AD and CN, MCI and CN, and MCI and AD. To perform these predictions, we independently evaluated each of these three predictions using a substantial number of features extracted during the initial stage, totaling 11,400 features for each image (120 x 95). It's crucial to note that having an excessive number of features can lead to overfitting, which is a common challenge in supervised machine learning[40]. To mitigate this issue, we employed feature reduction techniques aimed at reducing the feature count. The selection of an appropriate algorithm for feature reduction is a critical decision in the field of machine learning, as highlighted in reference[41]. Before applying the feature reduction methods to our extracted features, we first preprocessed these features. This preprocessing involved eliminating constant, quasi-

Preprints (www.preprints.org) | NOT PEER-REVIEWED | Posted: 8 November 2023 doi:10.20944/preprints202311.0513.v1

constant, and duplicated features. This step is essential for ensuring the quality of the feature set. With our preprocessed feature set, consisting of 5,351 features, we embarked on a comprehensive exploration of various dimension reduction methods to identify the most effective approach for our problem. Subsequently, we calculated the accuracy of each subset of the most significant features using a rank-based method. Throughout this comparison, we adhered to the default parameters as defined in the Scikit-learn library for all classifiers. We refrained from hyperparameter tuning, as our primary focus was on the feature reduction aspect of the machine learning process.

4.1. AD vs CN

The outcomes displayed in Table 2 reveal that among the various classifiers and feature selection methods evaluated, the Random Forest (RF) classifier with LASSO exhibited the most impressive performance, achieving a good accuracy with an Area Under the Curve (AUC) value of 0.976. This accuracy surpassed the performance of all other combinations of classifiers and feature selection techniques, underscoring the superiority of the RF classifier when applied to features selected via the LASSO method. This finding highlights the effectiveness of this specific combination in achieving high-quality results in our study.

Table 2. (Heatmap) Results of performing nine classifiers GB, RF, DT, GNB, GP, MLP, QDA, AB, and KNN on the top 20 features selected by eight dimension-reduction methods ANOVA, PCA, Chi-Square, LASSO, MI, RFA, FI, and RFE.

`	GB	RF	DT	GNB	GP	MLP	QDA	AB	KNN
ANOVA	0.957	0.962	0.85	0.961	0.91	0.935	0.958	0.951	0.912
PCA	0.92	0.929	0.784	0.919	0.677	0.853	0.918	0.904	0.79
Chi-Square	0.936	0.941	0.825	0.947	0.934	0.928	0.942	0.918	0.919
LASSO	0.971	0.976	0.874	0.971	0.914	0.919	0.972	0.967	0.909
MI	0.952	0.951	0.838	0.947	0.906	0.916	0.94	0.939	0.903
RFA	0.968	0.968	0.872	0.97	0.942	0.897	0.966	0.955	0.919
FI	0.949	0.955	0.838	0.955	0.92	0.941	0.952	0.933	0.921
RFE	0.959	0.964	0.853	0.965	0.899	0.939	0.955	0.943	0.927

Based on the data presented in Table 2, it's evident that the Random Forest (RF) classifier outperformed other classifiers and feature selection methods in terms of accuracy, achieving an impressive AUC of 0.976. This level of accuracy was notably higher than what was attained with alternative combinations of classifiers and feature selection techniques. To reach this result, we followed a specific process.

Initially, we applied the LASSO method to the preprocessed feature set, consisting of 5,351 features. Subsequently, we utilized a rank-based method, which leveraged the coefficients of the features, to calculate the average accuracy across all subsets of the top 20 features. This calculation was performed through 100 iterations, each using independent test data.

The RF classifier, when applied to features obtained via the LASSO algorithm and subjected to 100 iterations, demonstrated a high area under the curve (AUC) of 0.976, with a 95% confidence interval ranging from 0.95 to 0.98. This signifies the robustness and reliability of the RF classifier when working with these features of LASSO method.

Figure 2 provides a graphical representation of our findings. It illustrates that after including four features, there is minimal improvement in performance. These four Regions of Interest (ROIs) are isthmus cingulate (left hemisphere), inferior parietal (left hemisphere), hippocampus (left hemisphere), and entorhinal (right hemisphere). The selected features consist of

Preprints (www.preprints.org) | NOT PEER-REVIEWED | Posted: 8 November 2023 doi:10.20944/preprints202311.0513.v1

firstorder_90Percentile, firstorder_Median, glrlm_LongRunEmphasis, and gldm_DependenceEntropy.

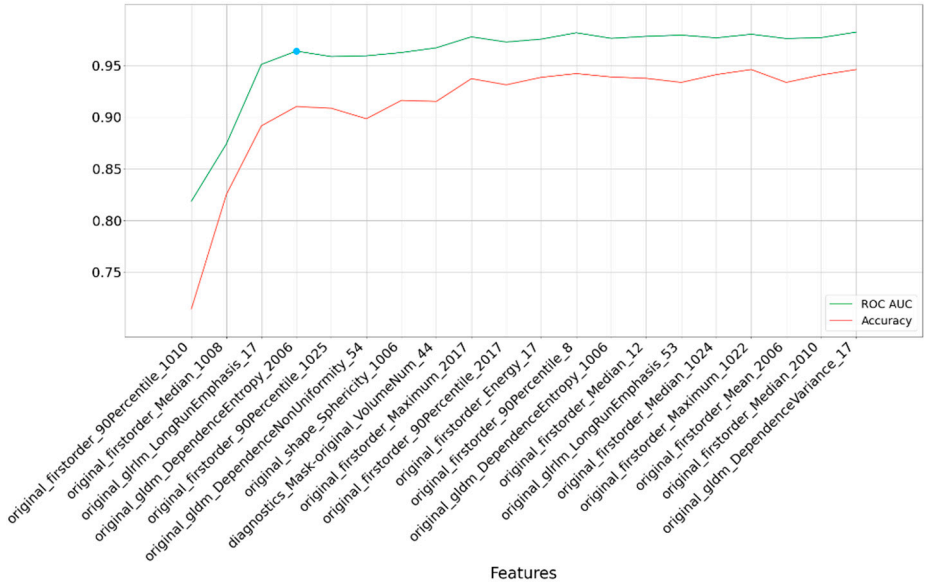

Figure 2. Rank-based results for each subset of the top 20 most important features selected by the LASSO method. The blue point is the optimal point based on accuracy and feature count. The last numbers of feature names are

Furthermore, leveraging the four most crucial features, we evaluated accuracy with a tuned classifier. Once the RF classification method was chosen and its hyperparameters fine-tuned using randomized-search cross-validation (with a 5-fold cross-validation), we achieved an AUC of 0.961 with 100 iterations and a 95% confidence interval spanning from 0.938 to 0.982. This further underscores the efficacy of the RF classifier in producing consistent and high-quality results for our classification model.

4.2. AD vs MCI

In the context of distinguishing between Alzheimer's Disease (AD) and Mild Cognitive Impairment (MCI), our analysis revealed that the Random Forest (RF) classifier, when applied to features selected through the LASSO method, delivered the highest level of accuracy. This achievement has shown in Table 3, where the classifier yielded an AUC of 0.917.

To carry out this prediction task for AD vs MCI, we initially applied LASSO to preprocessed feature set, containing 5,351 features. Subsequently, we employed a rank-based approach, focusing on the top 50 features and performing 100 iterations. Within this framework, the RF classifier consistently demonstrated acceptable performance, resulting in an average accuracy with an AUC of 0.917.

Further refinement of our analysis led us to identify the most critical features—six in total—based on their impact on accuracy, as illustrated in Figure 3. Even with this more concise feature set, the model exhibited commendable accuracy, resulting in an AUC of 0.862.

Table 3. (Heatmap) Results of performing nine classifiers GB, RF, DT, GNB, GP, MLP, QDA, AB and KNN on the top 50 features selected by the eight dimension-reduction methods ANOVA, PCA, Chi2, LASSO, MI, RFA, FI, and RFE to predict AD vs MCI.

`	GB	RF	DT	GNB	GP	MLP	QDA	AB	KNN
ANOVA	0.815	0.815	0.683	0.843	0.772	0.806	0.818	0.787	0.781
PCA	0.758	0.782	0.625	0.796	0.615	0.744	0.777	0.751	0.693

Preprints (www.preprints.org) | NOT PEER-REVIEWED | Posted: 8 November 2023 doi:10.20944/preprints202311.0513.v1

Chi-Square	0.781	0.813	0.668	0.83	0.836	0.812	0.804	0.768	0.796
LASSO	0.862	0.917	0.72	0.889	0.787	0.825	0.857	0.825	0.748
MI	0.843	0.837	0.698	0.828	0.793	0.798	0.815	0.826	0.793
RFA	0.872	0.862	0.724	0.871	0.791	0.799	0.845	0.851	0.782
FI	0.863	0.868	0.716	0.852	0.778	0.822	0.823	0.833	0.77
RFE	0.834	0.829	0.693	0.835	0.798	0.797	0.804	0.805	0.763

To improve the prediction accuracy, we pursued fine-tuning of the RF classifier's hyperparameters, which had a positive effect on the results. With these enhancements, the AUC increased to 0.874 with 100 iterations, and we can express our confidence in this outcome with a 95% confidence interval spanning from 0.822 to 0.912. This demonstrates the robustness and reliability of our predictive model in discerning between AD and MCI, providing valuable insights for clinical applications.

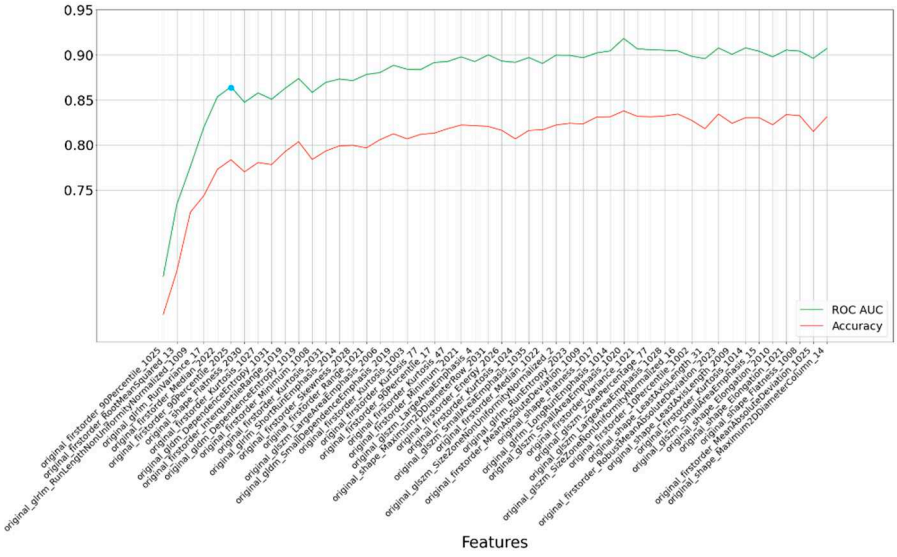

Figure 3. Rank-based results for each subset of the top 50 most important features selected by the LASSO method. The blue point is the optimal point based on accuracy and feature count. The last numbers of feature names are segmentation labels based on FastSurfer.

4.3. CN vs MCI

As indicated by the findings presented in Table 4, the Random Forest (RF) classifier consistently demonstrated the highest level of accuracy when applied to features selected through the LASSO method. This achievement was particularly notable during 100 iterations, yielding an AUC of 0.879. Furthermore, we can express our confidence in this result with a 95% confidence interval ranging from 0.747 to 0.911.

In our quest to assess the average accuracy in distinguishing between Cognitively Normal (CN) and Mild Cognitive Impairment (MCI), we adopted a rank-based approach focusing on the top 80 features, executing 100 iterations for each subset of features. Within this framework, the RF classifier consistently exhibited robust performance, achieving an average accuracy with an AUC of 0.879.

Our analysis further led us to identify the most influential features—eight in total—based on their impact on accuracy, as visually represented in Figure 4. Even with this more refined feature set, the model maintained a commendable level of accuracy, resulting in an AUC of 0.778, as depicted in Table 5.

Preprints (www.preprints.org) | NOT PEER-REVIEWED | Posted: 8 November 2023 doi:10.20944/preprints202311.0513.v1

Table 4. (Heatmap) Results of performing nine classifiers GB, RF, DT, GNB, GP, MLP, QDA, AB and KNN on the top 80 features selected by the eight dimension-reduction methods ANOVA, PCA, Chi2, LASSO, MI, RFA, FI, and RFE to predict CN vs MCI.

`	GB	RF	DT	GNB	GP	MLP	QDA	AB	KNN
ANOVA	0.849	0.878	0.635	0.791	0.693	0.635	0.641	0.847	0.695
PCA	0.862	0.875	0.651	0.771	0.596	0.57	0.625	0.854	0.582
Chi-Square	0.798	0.809	0.643	0.779	0.658	0.603	0.583	0.785	0.622
LASSO	0.861	0.879	0.631	0.754	0.692	0.684	0.645	0.858	0.695
MI	0.787	0.793	0.635	0.785	0.649	0.659	0.648	0.767	0.646
RFA	0.821	0.827	0.664	0.791	0.554	0.567	0.665	0.792	0.627
FI	0.802	0.814	0.635	0.775	0.6	0.597	0.676	0.786	0.646
RFE	0.787	0.799	0.638	0.791	0.547	0.631	0.681	0.746	0.68

Table 5. Important Features and ROIs selected by the LASSO method

	Feature Name	ROI Id	ROI Name	Left/Right
CN vs AD	firstorder_90Percentile	1010	isthmuscingulate	lh
	firstorder_Median	1008	inferiorparietal	lh
	glrlm_LongRunEmphasis	17	Hippocampus	lh
	gldm_DependenceEntropy	2006	entorhinal	rh
AD Vs MCI	firstorder_90Percentile	1025	precuneus	lh
	firstorder_RootMeanSquared	13	Pallidum	lh
	glrlm_RunLengthNonUniformityNormalized	1009	inferiortemporal	lh
	glrlm_RunVariance	17	Hippocampus	lh
	firstorder_Median	2022	postcentral	rh
	firstorder_90Percentile	2025	precuneus	rh
CN Vs MCI	firstorder_Maximum	16	Brain Stem	
	firstorder_90Percentile	2008	inferiorparietal	rh
	gldm_DependenceVariance	2012	lateralorbitofrontal	rh
	glszm_ZonePercentage	1022	postcentral	lh
	firstorder_Minimum	2035	insula	rh
	shape_Maximum2DDiameterColumn	2020	parstriangularis	rh
	shape_Sphericity	28	Ventral DC	lh
	glrlm_ShortRunEmphasis	10	Thalamus	lh

We then embarked on the fine-tuning of the RF classifier's hyperparameters, specifically for the top features (eight in total). This fine-tuning effort yielded an average value for the area under the ROC curve (0.79) after 100 iterations. Our confidence in this result is substantiated by a 95% confidence interval spanning from 0.753 to 0.861. These findings underscore the model's robustness and reliability in distinguishing between CN and MCI, carrying significant implications for clinical applications and research.

Preprints (www.preprints.org) | NOT PEER-REVIEWED | Posted: 8 November 2023 doi:10.20944/preprints202311.0513.v1

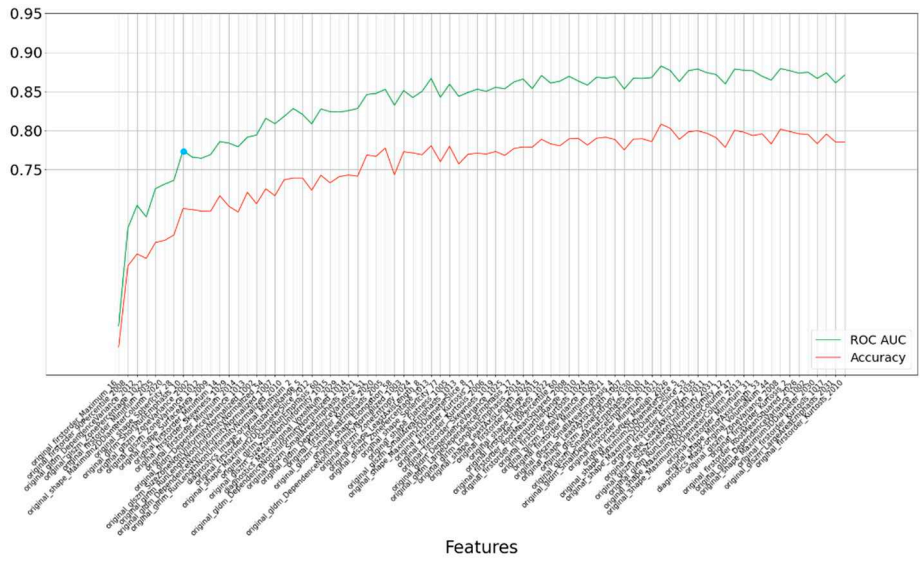

Figure 4. Rank-based results for each subset of the top 80 most important features selected by the LASSO method. The blue point is the optimal point based on accuracy and feature count. The last numbers of feature names are segmentation labels based on FastSurfer.

5. Discussion

In this study, our primary focus was on diagnosing Alzheimer's Disease (AD) and Mild Cognitive Impairment (MCI) by developing a radiomics-based platform known as RAB-PET. We also devised a method to analyze 18FDG-PET brain images in patients with AD and MCI. Early diagnosis of AD is a critical strategy in the context of preventing and treating this debilitating condition. This early diagnosis relies on the measurement of specific characteristics in distinct regions of the human brain, as noted in reference[42]. Our platform, RAB-PET, provides us with the capability to uncover effective radiomics solutions by exploring nine different classification methods in conjunction with eight diverse feature selection methods, all utilizing 18FDG-PET images. Significantly, in contrast to recent research endeavors as outlined in Table 3, our method demonstrated a notably elevated level of accuracy. Specifically, we achieved an AUC of 0.976 for the AD vs CN, an AUC of 0.917 for the AD vs MCI, and an AUC of 0.879 for MCI vs CN. It's important to acknowledge that direct comparisons with these studies are somewhat constrained due to variations in the datasets and biomarkers used.

For the crucial task of volume analysis, we employed FastSurfer, a novel approach based on deep learning. FastSurfer facilitated the segmentation of the entire brain into 95 distinct classes, drawing upon the DKT atlas. This method offered an efficient alternative to time-consuming brain segmentation techniques like FreeSurfer, Statistical Parametric Mapping (SPM), or FSL, as elaborated in reference[43]. In addition, we harnessed PyRadiomics, which performed the computation of 2D and 3D properties according to the IBSI standard[44,45].

To the best of our knowledge, the developed platform is the first capable of generating multiple outcomes while leveraging specialized hardware and 18FDG-PET studies. It's worth emphasizing that 18FDG-PET, recognized for its sensitivity, stands out as the foremost diagnostic imaging method for Alzheimer's Disease (AD), as established by reference[46]. This imaging technique proves to be of immense value, particularly in the early phases of the disease since metabolic change occur much earlier than the symptoms.

In the existing literature, several studies have explored the potential of structural MRI (sMRI) scans for predicting Alzheimer's Disease (AD) or Mild Cognitive Impairment (MCI), as referenced in[47,48]. It's noteworthy that many recent investigations have adopted a multi-faceted approach, combining various biomarkers, including clinical tests and diverse imaging modalities, to enhance the accuracy of AD and MCI predictions, as indicated by[49]. In contrast, our approach was more streamlined, relying exclusively on 18FDG-PET.

 doi:10.20944/preprints202311.0513.v1

After extracting features from 18FDG-PET scans, we took measures to optimize computation time. This involved preprocessing the features and selecting the top 'n' features for each prediction task, where 'n' was determined as follows: for CN vs. AD, we used 'n=20', for AD vs. MCI, 'n=50', and for CN vs. MCI, 'n=80'. This reduction in feature set size aimed to enhance efficiency while maintaining the predictive power of our approach. Furthermore, for the sake of result interpretability, we went a step further by selecting the most vital features based on their contribution to accuracy and feature count. For CN vs. AD, we retained 'n=4' critical features, for AD vs. MCI, 'n=6', and for CN vs. MCI, 'n=6'. This step not only enhanced the practical utility of our predictions but also facilitated a better understanding of the underlying factors driving our diagnostic capabilities in different scenarios.

It's important to highlight that particular regions of interest (ROIs) that show early tau deposition can be valuable in aiding the early detection of Alzheimer's disease (AD)[50]. Moreover, as per the National Institute on Aging (NIH) report, Alzheimer's disease initially damages neurons and their connections in brain regions associated with memory, later extending its impact to the cerebral cortex areas responsible for language, cognition, and social behavior[51]. Efforts are being made to link these regions with the areas identified through radiomic analysis.

In our study, we discovered that various prediction models exhibit a preference for different brain regions and features. However, in our quest to identify shared elements among these distinct prediction scenarios, we conducted an extensive analysis. This analysis revealed a remarkable and consistent finding: the amygdala, entorhinal cortex, and hippocampus consistently emerged as pivotal regions across all stages of Alzheimer's disease. These three brain regions, known for their roles in memory and cognitive function, demonstrated their enduring significance in our predictive model. This finding suggests that, regardless of the specific predictive task or feature selection method, the amygdala, entorhinal cortex, and hippocampus remain robust markers that hold vital relevance throughout the progression of Alzheimer's disease. This insight has the potential to enhance the accuracy and consistency of diagnostic and predictive models, ultimately contributing to our understanding and management of this disease.

Furthermore, an additional discovery from our study is the identification of four frequently employed features (namely, gldm_DependenceEntropy, shape_SurfaceVolumeRatio, glrlm_RunPercentage, glrlm_LongRunEmphasis) by eight distinct feature selection methods. These features were consistently recognized as the most critical in predicting Alzheimer's disease (AD) within three specific Regions of Interest (ROIs): the amygdala, entorhinal cortex, and hippocampus (as depicted in Figure 5). Given the relatively limited size of these identified areas, as depicted in Figure 6, visual assessment and the ability to discern changes with the naked eye are challenging. As a result, machine learning techniques prove invaluable in quantifying and analyzing features within these regions, offering medical experts valuable and practical insights into these highlighted areas.

Considering recent clinical studies on patients with AD, it can be concluded that these three ROIs are the most affected parts of the brain related to AD. A recent study introduced the entorhinal, amygdala, and parahippocampal regions as early tau-deposited regions of temporal meta-ROI, which can assist in the early diagnosis of AD disease[50]. In addition, according to the report of the National Institute on Aging (NIH), Alzheimer's disease typically destroys neurons and their connections in parts of the brain involved in memory, including the entorhinal cortex and hippocampus. It later affects areas in the cerebral cortex responsible for language, reasoning, and social behavior[51].

Preprints (www.preprints.org) | NOT PEER-REVIEWED | Posted: 8 November 2023 doi:10.20944/preprints202311.0513.v1

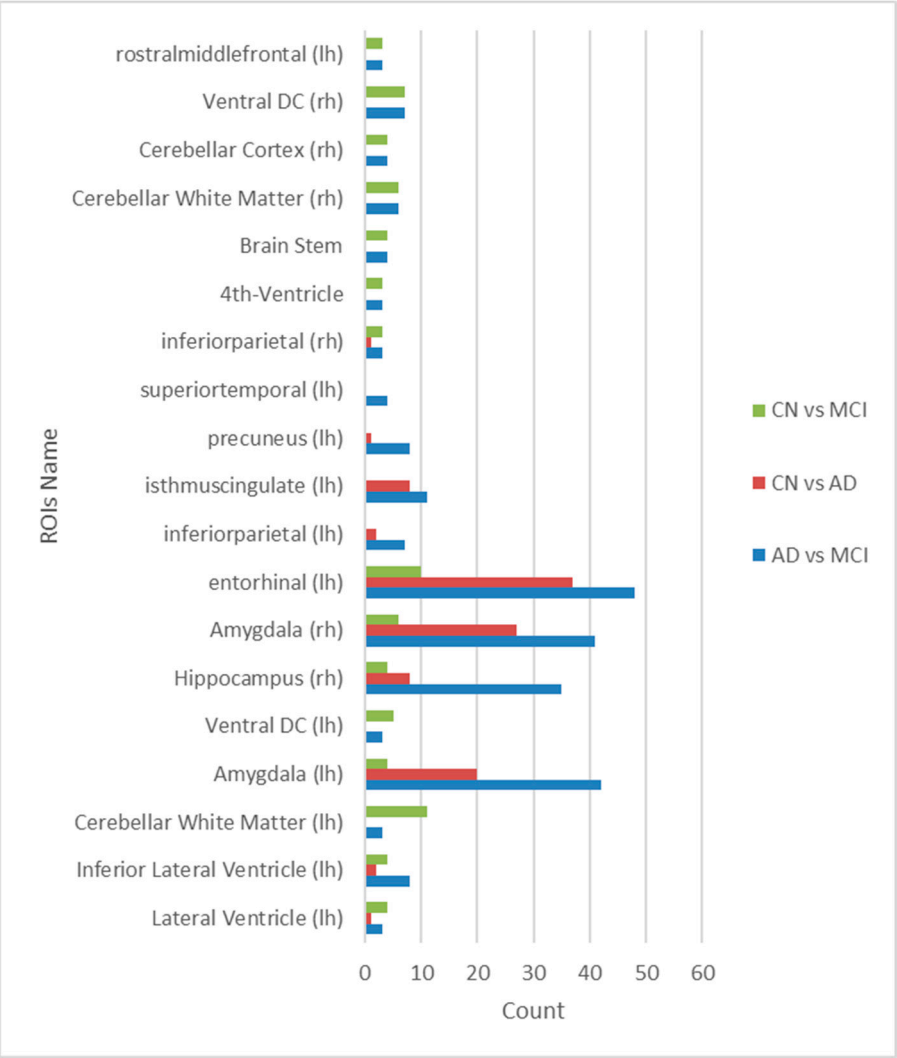

Figure 5. Common ROIs frequently selected by eight different feature selection methods.

Preprints (www.preprints.org) | NOT PEER-REVIEWED | Posted: 8 November 2023 doi:10.20944/preprints202311.0513.v1

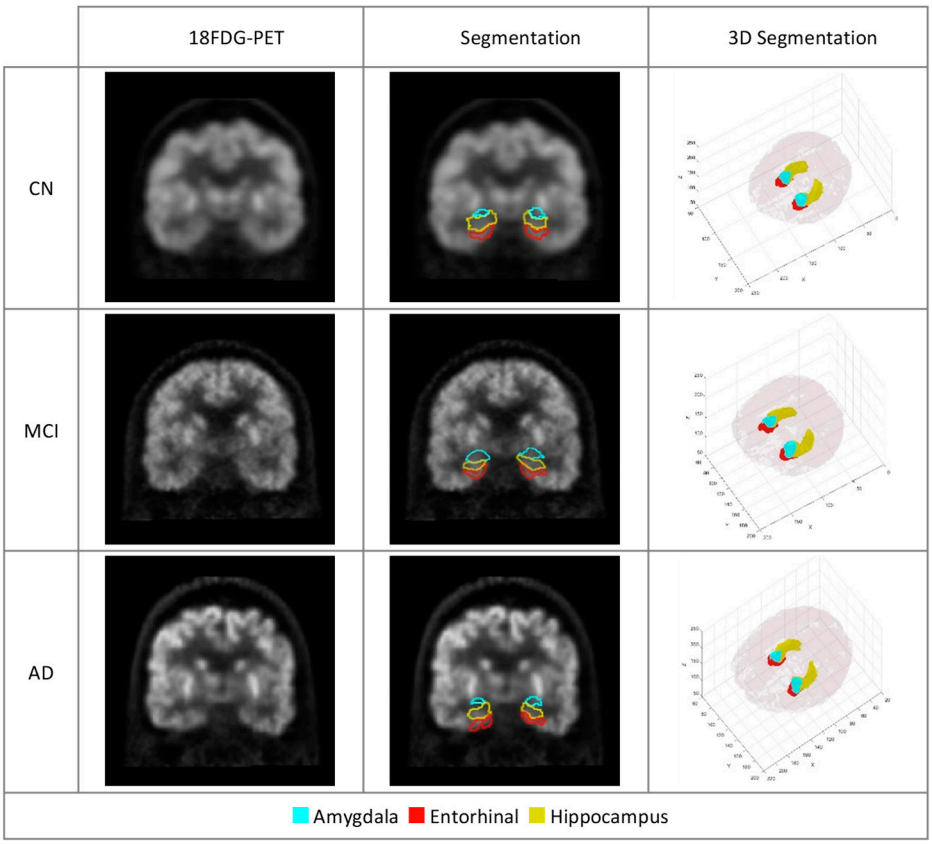

Figure 6. 18FDGPET scans of participants with AD, MCI and CN. The marked regions of the three ROIs important in the diagnosis of AD introduced by our model.

Another finding of this study is to show how the classification and the feature reduction methods affect the results. We investigated nine classification methods on the eight different feature selection methods to find the best combination of feature selection and classification methods. We found that LASSO is a well-performing feature selection method with the RF classifier in 18FDG-PET images.

Despite the promising results of radiomics in various fields of medicine and its potential application in precision medicine[52], deep exploration, refinement, standardization, and validation are still required for application in clinical practice[53]. Therefore, validating the proposed models by further studies is a necessary step that requires the provision of a comprehensive and standard solution to verify them for use in clinical practice. Moreover, many factors influence the outcomes of the radiomics approach, so this field relies on the performance of different methods, such as segmentation, feature extraction, and classification[54].

Our study confirms that 18FDG-PET can be an important biomarker for AD in comparison with recent studies as shown in Table 6. We believe that the predictive performance of the proposed solution can be improved by extending the dataset size or combining it with other existing datasets. Our model is a general method that does not consider specific prior information about regions of interest or disease symptoms. Therefore, in future work, it can be applied to predict other neurological diseases or to predict other quantitative characteristics of AD[55].

Table 6. Comparison of our results with related published studies on the classification of AD

Preprints (www.preprints.org) | NOT PEER-REVIEWED | Posted: 8 November 2023 doi:10.20944/preprints202311.0513.v1

Year	Author	Dataset Size				CN vs AD		CN vs MCI		MCI vs AD		Algorithm	Segmentation	Database	Modality
		Total	CN	AD	MCI	Acc (%)	AUC	Acc (%)	AUC	Acc (%)	AUC				
2023	Zhigeng Chen	159	53	51	55	0.97	0.98	0.86	0.81	0.85	0.85	Logistic Regression (LR)	SPM12	ADNI	FDG PET/MRI
2022	Yüksel, C	157	132	125	-	-	0.96	-	-	-	-	Similarity Index + KNN	-	ADNI	FDG PET
2021	Katia M. Poloni	762	302	209	251	89.24	0.95	75.58	0.83	69.8	0.73	SVM	FSL	ADNI, NAC-IXI	sMRI
2020	Chunfeng Lian	787	429	358	-	90.3	0.95	-	-	-	-	DL (hierarchical fully convolutional network)	-	ADNI	sMRI
2020	M. Liu	449	119	97	233	88.9	0.93	76.2	0.78	-	-	DL (CNN)	-	ADNI	sMRI
2018	Liu	787	429	358	-	91.09	0.96	-	-	-	-	Deep multi-instance learning	landmark-based	ADNI, MIRIAD	sMRI
2017	J. Zhang	1191	201	159	831	83.7	-	73.6	-	-	-	SVM	landmark-based	ADNI	sMRI
2017	Sergey Korolev	231	61	50	120	79	0.88	63	0.67	62	0.61	DL (CNN)	-	ADNI	sMRI
2017	Jun Zhang	707	207	154	346	88.3	0.94	79.02	0.85	-	-	SVM	landmark-based	ADNI	sMRI
2017	Peng Cao	818	229	192	397	88.6	0.9	71.9	0.73	-	-	Multiple kernel learning (MKL)	Freesurfer	ADNI	sMRI
2016	Tingting Ye	202	52	51	99	87.26	0.93	68.02	0.71	-	-	Multi-modality based	-	ADNI	FDG PET/MRI
2014	Siqi Liu	311	77	65	169	87.76	-	76.92	-	-	-	Multiple classes	-	ADNI	sMRI
Proposed Method		***549***	***188***	***163***	***198***	***94.8***	***0.98***	***80.9***	***0.88***	***87.9***	***0.91***	***Random Forest (RF)***	***Fastsurfer***	***ADNI***	***FDG PET***

6. Conclusion

In summary, the developed RAB-PET platform offers an efficient solution for the radiomic analysis of brain FDG-PET images. Testing on AD and MCI patients has shown its potential for reliable AD diagnosis and identification of its stages, accomplished with minimal computational time. It also helps the identification of the few most important regions and features associated with the disease. Furthermore, we're actively exploring its applications in personalized AD management, and its adaptable nature extends its usability to predict various other brain disorders.

Acknowledgments: We gratefully acknowledge the financial support provided by Bogazici University Research Fund (BAP) for this research under project code 19774. Their support was instrumental in carrying out the experiments and analyzing the data. Data collection and sharing for this project was funded by the Alzheimer's Disease Neuroimaging Initiative (ADNI) (National Institutes of Health Grant U01 AG024904) and DOD ADNI (Department of Defense award number W81XWH-12-2-0012). ADNI is funded by the National Institute on Aging, the National Institute of Biomedical Imaging and Bioengineering, and through generous contributions from the following: AbbVie, Alzheimer's Association; Alzheimer's Drug Discovery Foundation; Araclon Biotech; BioClinica, Inc.; Biogen; Bristol-Myers Squibb Company; CereSpir, Inc.; Cogstate; Eisai Inc.; Elan Pharmaceuticals, Inc.; Eli Lilly and Company; EuroImmun; F. Hoffmann-La Roche Ltd and its affiliated company Genentech, Inc.; Fujirebio; GE Healthcare; IXICO Ltd.; Janssen Alzheimer Immunotherapy Research & Development, LLC.; Johnson & Johnson Pharmaceutical Research & Development LLC.; Lumosity; Lundbeck; Merck & Co., Inc.; Meso Scale Diagnostics, LLC.; NeuroRx Research; Neurotrack Technologies; Novartis Pharmaceuticals Corporation; Pfizer Inc.; Piramal Imaging; Servier; Takeda Pharmaceutical Company; and Transition Therapeutics. The Canadian Institutes of Health Research is providing funds to support ADNI clinical

sites in Canada. Private sector contributions are facilitated by the Foundation for the National Institutes of Health (www.fnih.org). The grantee organization is the Northern California Institute for Research and Education, and the study is coordinated by the Alzheimer's Therapeutic Research Institute at the University of Southern California. ADNI data are disseminated by the Laboratory for Neuro Imaging at the University of Southern California.

References

1. 2020 Alzheimer's disease facts and figures. *Alzheimer's and Dementia* **16**, 391–460 (2020).
2. *World Alzheimer Report 2023 Reducing dementia risk: never too early, never too late*.
3. Younes, L. *et al.* Identifying changepoints in biomarkers during the preclinical phase of Alzheimer's disease. *Front Aging Neurosci* **11**, (2019).
4. Grill, J. D., Cox, C. G., Harkins, K. & Karlawish, J. Reactions to learning a 'not elevated' amyloid PET result in a preclinical Alzheimer's disease trial. *Alzheimers Res Ther* **10**, (2018).
5. Revathi, A. *et al.* Early Detection of Cognitive Decline Using Machine Learning Algorithm and Cognitive Ability Test. *Security and Communication Networks* **2022**, 1–13 (2022).
6. Verma, R. K. *et al.* An Insight into the Role of Artificial Intelligence in the Early Diagnosis of Alzheimer's Disease. *CNS Neurol Disord Drug Targets* **21**, 901–912 (2022).
7. Guiot, J. *et al.* A review in radiomics: Making personalized medicine a reality via routine imaging. *Med Res Rev* **42**, 426–440 (2022).
8. Chételat, G. *et al.* Amyloid-PET and 18F-FDG-PET in the diagnostic investigation of Alzheimer's disease and other dementias. *Lancet Neurol* **19**, 951–962 (2020).
9. Mannil, M., von Spiczak, J., Manka, R. & Alkadhi, H. Texture Analysis and Machine Learning for Detecting Myocardial Infarction in Noncontrast Low-Dose Computed Tomography. *Invest Radiol* **53**, 338–343 (2018).
10. Li, Y. *et al.* Radiomics: a novel feature extraction method for brain neuron degeneration disease using ^{18}F-FDG PET imaging and its implementation for Alzheimer's disease and mild cognitive impairment. *Ther Adv Neurol Disord* **12**, 175628641983868 (2019).
11. Zanfardino, M. *et al.* Bringing radiomics into a multi-omics framework for a comprehensive genotype–phenotype characterization of oncological diseases. *J Transl Med* **17**, 337 (2019).
12. Zwanenburg, A. *et al.* The Image Biomarker Standardization Initiative: Standardized Quantitative Radiomics for High-Throughput Image-based Phenotyping. *Radiology* **295**, 328–338 (2020).
13. Henschel, L. *et al.* FastSurfer - A fast and accurate deep learning based neuroimaging pipeline. *Neuroimage* **219**, 117012 (2020).
14. Fischl, B. FreeSurfer. *Neuroimage* **62**, 774–781 (2012).
15. Rasi, R. & Guvenis, A. A Platform for the Radiomic Analysis of Brain FDG PET Images: Detecting Alzheimer's Disease. in *International Work-Conference on Bioinformatics and Biomedical Engineering* 244–255 (2023).
16. Li, Y., Jiang, J., Shen, T., Wu, P. & Zuo, C. Radiomics features as predictors to distinguish fast and slow progression of Mild Cognitive Impairment to Alzheimer's disease. in *2018 40th Annual International Conference of the IEEE Engineering in Medicine and Biology Society (EMBC)* 127–130 (IEEE, 2018). doi:10.1109/EMBC.2018.8512273.
17. Feng, Q. *et al.* Correlation Between Hippocampus MRI Radiomic Features and Resting-State Intrahippocampal Functional Connectivity in Alzheimer's Disease. *Front Neurosci* **13**, (2019).
18. Wang, L. *et al.* Textural features reflecting local activity of the hippocampus improve the diagnosis of Alzheimer's disease and amnestic mild cognitive impairment: A radiomics study based on functional magnetic resonance imaging. *Front Neurosci* **16**, (2022).
19. Feng, Q. *et al.* Comprehensive classification models based on amygdala radiomic features for Alzheimer's disease and mild cognitive impairment. *Brain Imaging Behav* **15**, 2377–2386 (2021).
20. Chen, Z. *et al.* Early Diagnosis of Alzheimer's Disease using Multiparametric Hippocampal Signatures with 18F-FDG PET/MR Radiomics. Preprint at (2023).
21. Hu, J. *et al.* Diagnostic performance of magnetic resonance imaging–based machine learning in Alzheimer's disease detection: a meta-analysis. *Neuroradiology* **65**, 513–527 (2023).
22. Kim, D. W., Jang, H. Y., Kim, K. W., Shin, Y. & Park, S. H. Design Characteristics of Studies Reporting the Performance of Artificial Intelligence Algorithms for Diagnostic Analysis of Medical Images: Results from Recently Published Papers. *Korean J Radiol* **20**, 405 (2019).

23. Peng, J. *et al.* 18F-FDG-PET Radiomics Based on White Matter Predicts The Progression of Mild Cognitive Impairment to Alzheimer Disease: A Machine Learning Study. *Acad Radiol* **30**, 1874–1884 (2023).
24. Shaffer, J. L. *et al.* Predicting Cognitive Decline in Subjects at Risk for Alzheimer Disease by Using Combined Cerebrospinal Fluid, MR Imaging, and PET Biomarkers. *Radiology* **266**, 583–591 (2013).
25. Jagust, W. J. *et al.* The Alzheimer's Disease Neuroimaging Initiative 2 PET Core: 2015. *Alzheimer's & Dementia* **11**, 757–771 (2015).
26. van Griethuysen, J. J. M. *et al.* Computational Radiomics System to Decode the Radiographic Phenotype. *Cancer Res* **77**, e104–e107 (2017).
27. Ray, P., Reddy, S. S. & Banerjee, T. Various dimension reduction techniques for high dimensional data analysis: a review. *Artif Intell Rev* **54**, 3473–3515 (2021).
28. Salam, M. A., Taher, A., Samy, M. & Mohamed, K. The Effect of Different Dimensionality Reduction Techniques on Machine Learning Overfitting Problem. *International Journal of Advanced Computer Science and Applications* **12**, (2021).
29. Jović, A., Brkić, K. & Bogunović, N. A review of feature selection methods with applications. in *2015 38th international convention on information and communication technology, electronics and microelectronics (MIPRO)* 1200–1205 (2015).
30. Massafra, R. *et al.* Radiomic feature reduction approach to predict breast cancer by contrast-enhanced spectral mammography images. *Diagnostics* **11**, 684 (2021).
31. Mayerhoefer, M. E. *et al.* Introduction to radiomics. *Journal of Nuclear Medicine* **61**, 488–495 (2020).
32. Shu, Z. *et al.* MRI-based Radiomics nomogram to detect primary rectal cancer with synchronous liver metastases. *Sci Rep* **9**, 3374 (2019).
33. Muthukrishnan, R. & Rohini, R. LASSO: A feature selection technique in predictive modeling for machine learning. in *2016 IEEE international conference on advances in computer applications (ICACA)* 18–20 (2016).
34. Henriques, A. D., Benedet, A. L., Camargos, E. F., Rosa-Neto, P. & Nóbrega, O. T. Fluid and imaging biomarkers for Alzheimer's disease: Where we stand and where to head to. *Exp Gerontol* **107**, 169–177 (2018).
35. Probst, P., Boulesteix, A.-L. & Bischl, B. Tunability: Importance of hyperparameters of machine learning algorithms. *The Journal of Machine Learning Research* **20**, 1934–1965 (2019).
36. Elgeldawi, E., Sayed, A., Galal, A. R. & Zaki, A. M. Hyperparameter Tuning for Machine Learning Algorithms Used for Arabic Sentiment Analysis. *Informatics* **8**, 79 (2021).
37. Bogowicz, M. *et al.* Post-radiochemotherapy PET radiomics in head and neck cancer–the influence of radiomics implementation on the reproducibility of local control tumor models. *Radiotherapy and Oncology* **125**, 385–391 (2017).
38. Zwanenburg, A. *et al.* The image biomarker standardization initiative: standardized quantitative radiomics for high-throughput image-based phenotyping. *Radiology* **295**, 328–338 (2020).
39. Rasi Ramin & Guvenis Albert. RAB-PET. (2023) doi:10.5281/zenodo.7859694.
40. Ying, X. An Overview of Overfitting and its Solutions. *J Phys Conf Ser* **1168**, 022022 (2019).
41. Ray, P., Reddy, S. S. & Banerjee, T. Various dimension reduction techniques for high dimensional data analysis: a review. *Artif Intell Rev* **54**, 3473–3515 (2021).
42. Franceschi, A. M. & Franceschi, D. *Hybrid PET/MR Neuroimaging: A Comprehensive Approach*. (Springer Nature, 2021).
43. Palumbo, L. *et al.* Evaluation of the intra- and inter-method agreement of brain MRI segmentation software packages: A comparison between SPM12 and FreeSurfer v6.0. *Physica Medica* **64**, 261–272 (2019).
44. Zwanenburg, A. *et al.* The image biomarker standardization initiative: standardized quantitative radiomics for high-throughput image-based phenotyping. *Radiology* **295**, 328–338 (2020).
45. Bogowicz, M. *et al.* Post-radiochemotherapy PET radiomics in head and neck cancer–the influence of radiomics implementation on the reproducibility of local control tumor models. *Radiotherapy and Oncology* **125**, 385–391 (2017).
46. Wabik, A. *et al.* Comparison of dynamic susceptibility contrast enhanced MR and FDG-PET brain studies in patients with Alzheimer's disease and amnestic mild cognitive impairment. *J Transl Med* **20**, 1–14 (2022).
47. Basaia, S. *et al.* Automated classification of Alzheimer's disease and mild cognitive impairment using a single MRI and deep neural networks. *Neuroimage Clin* **21**, 101645 (2019).
48. Syaifullah, A. H. *et al.* Machine learning for diagnosis of AD and prediction of MCI progression from brain MRI using brain anatomical analysis using diffeomorphic deformation. *Front Neurol* **11**, 576029 (2021).

49. Gupta, Y., Lama, R. K., Kwon, G.-R. & Initiative, A. D. N. Prediction and classification of Alzheimer's disease based on combined features from apolipoprotein-E genotype, cerebrospinal fluid, MR, and FDG-PET imaging biomarkers. *Front Comput Neurosci* **13**, 72 (2019).
50. Cai, Y. *et al.* Initial levels of β-amyloid and tau deposition have distinct effects on longitudinal tau accumulation in Alzheimer's disease. *Alzheimers Res Ther* **15**, 30 (2023).
51. 2023 Alzheimer's disease facts and figures. *Alzheimer's & Dementia* **19**, 1598–1695 (2023).
52. Ardakani, A. A., Bureau, N. J., Ciaccio, E. J. & Acharya, U. R. Interpretation of radiomics features–a pictorial review. *Comput Methods Programs Biomed* **215**, 106609 (2022).
53. Frix, A.-N. *et al.* Radiomics in lung diseases imaging: state-of-the-art for clinicians. *J Pers Med* **11**, 602 (2021).
54. Yip, S. S. F. & Aerts, H. J. W. L. Applications and limitations of radiomics. *Phys Med Biol* **61**, R150–R166 (2016).
55. Zhang, J., Gao, Y., Gao, Y., Munsell, B. C. & Shen, D. Detecting anatomical landmarks for fast Alzheimer's disease diagnosis. *IEEE Trans Med Imaging* **35**, 2524–2533 (2016).